

A comparative analysis of the observed white dwarf cooling sequence from globular clusters

Fabíola Campos^{1*}, P. Bergeron², A.D. Romero¹, S. O. Kepler¹, G. Ourique¹,
J. E. S. Costa¹, C. J. Bonatto¹, D. E. Winget³, M. H. Montgomery³, T. A. Pacheco¹,
L. R. Bedin⁴

¹*Departamento de Astronomia, Universidade Federal do Rio Grande do Sul, Av. Bento Gonçalves 9500 Porto Alegre 91501-970, RS, Brazil*

²*Département de Physique, Université de Montréal, C.P. 6128, Succursale Centre-Ville, Montréal, Québec H3C 3J7, Canada*

³*Department of Astronomy, University of Texas at Austin, Austin, TX, USA*

⁴*Istituto Nazionale di Astrofisica, Osservatorio Astronomico di Padova, Vicolo dell' Osservatorio 5, Padova, IT-35122, Italy*

Accepted 2015 December 8. Received 2015 December 3; in original form 2015 August 11

ABSTRACT

We report our study of features at the observed red end of the white dwarf cooling sequences for three Galactic globular clusters: NGC 6397, 47 Tucanae and M 4. We use deep colour-magnitude diagrams constructed from archival Hubble Space Telescope (ACS) to systematically investigate the blue turn at faint magnitudes and the age determinations for each cluster. We find that the age difference between NGC 6397 and 47 Tuc is $1.98^{+0.44}_{-0.26}$ Gyr, consistent with the picture that metal-rich halo clusters were formed later than metal-poor halo clusters. We self-consistently include the effect of metallicity on the progenitor age and the initial-to-final mass relation. In contrast with previous investigations that invoked a single white dwarf mass for each cluster, the data shows a spread of white dwarf masses that better reproduce the shape and location of the blue turn. This effect alone, however, does not completely reproduce the observational data - the blue turn retains some mystery. In this context, we discuss several other potential problems in the models. These include possible partial mixing of H and He in the atmosphere of white dwarf stars, the lack of a good physical description of the collision-induced absorption process and uncertainties in the opacities at low temperatures. The latter are already known to be significant in the description of the cool main sequence. Additionally, we find that the present day local mass function of NGC 6397 is consistent with a top-heavy type, while 47 Tuc presents a bottom-heavy profile.

Key words: (*The Galaxy:*) globular clusters: general, globular clusters: individual, (*stars:*) white dwarfs, stars: evolution

1 INTRODUCTION

Galactic globular clusters are among the largest and oldest stellar systems in the Milky Way. They contain thousands to millions of stars at approximately the same distance from the Sun: their cluster half-light radii are ~ 4 pc (e.g. Bonatto et al. 2007) while their distances are larger than 2 kpc (Harris 1996). The stars forming the globular clusters are considered excellent laboratories to study stellar evolution. They are assumed to be part of a simple stellar population, meaning that all stars have been formed at essentially the same time, from the same cloud and have the

same initial chemical composition (Moehler & Bono 2008). More precise investigations have shown that most of the globular clusters are not composed of a simple stellar population; instantaneous star formation and complete chemical homogeneity of the original cloud should not be expected (e.g. D’Antona et al. 2005; Piotto et al. 2015). An extreme case is that of ω Centauri, which clearly has multiple main sequences (Bedin et al. 2004) and a double white dwarf cooling sequence (Bellini et al. 2013). However, such features are not so extreme. Nevertheless, globular clusters remain excellent laboratories, composed of stars from the central hydrogen-burning limit in the main sequence to cool white dwarf stars.

The white dwarf phase is the evolutionary end-

* fabiola.campos@ufrgs.br

point of stars with initial masses lower than roughly $10 M_{\odot}$ (e.g. Ibeling & Heger 2013; Doherty et al. 2015). Thus they represent the collective fate of $\sim 97\%$ of the stars (e.g. Fontaine, Brassard & Bergeron 2001). Moehler & Bono (2008) argue that white dwarf stars in clusters offer an advantage over field white dwarf stars in that they provide the opportunity to constrain the initial-to-final mass relation. Besides, most of the globular clusters are mono-metallic systems with respect to iron, with a minimum spread in age. Moreover, the local densities of the halo, thick, and thin disk white dwarf populations are lower than their local density in a globular cluster, making it possible to observe large samples of white dwarfs without the need for wide-field surveys. There are several substantial obstacles in the study of white dwarf stars in globular clusters: they are more distant than the neighbouring stars, the effect of crowding is significant and white dwarf stars are very faint, requiring deep photometric observations with high quality. In that context, Hansen (1998) pointed out that only when it were possible to examine the faint white dwarf stars in globular clusters it would be possible to empirically test the effects of advanced age and low-metallicity progenitors. The globular clusters NGC 6397, 47 Tuc and M 4 are the first ones that have data reaching the red end of the white dwarf cooling sequence, thus providing the means to study stellar evolution and the coolest observable white dwarf stars in globular clusters in an unprecedented way.

The pioneering results achieved by Richer et al. (2006) with deep HST/ACS of NGC 6397 showed, for the first time, the colour-magnitude diagram of a globular cluster down to the main sequence hydrogen-burning limit, and pointed the existence of a red cut-off in the white dwarf cooling sequence at $m_{F814W}=27.8$. Using artificial star tests and star-galaxy separation, Hansen et al. (2007) demonstrated that the cut-off represents a real truncation of the white dwarf stars luminosity function and estimated the age of NGC 6397 to be 11.47 ± 0.47 Gyr. More recently, with the same method, Hansen et al. (2013) determined the age of the metal rich globular cluster 47 Tuc as being 9.90 ± 0.70 Gyr, finding that this cluster is approximately 2 Gyr younger than NGC 6397. However, García-Berro et al. (2014) determined an age of ~ 12.00 Gyr for 47 Tuc, also using the cooling sequence method but with different models. This brought up questions about the reliability of ages determined through the white dwarf cooling sequence (Forbes et al. 2015) and the importance of the theoretical evolutionary models used.

When Hansen et al. (2007) compared their best fit model to the data, they noticed that the only features of the observations that were not well reproduced by their best fit models were the blue colours at magnitudes around $F814W=27.25$, indicating a mismatch between theoretical and true colours at the faintest temperatures ($T_{\text{eff}} \sim 5000$ K). They argued that the mismatch between models and data indicated either residual deficiencies in the models or that the atmospheres could be composed of a mixture of hydrogen and helium. They also proposed that the blue turn in the colours was driven by collision-induced absorption of molecular hydrogen, a significant effect on environments composed of molecules or dense, neutral and non-polar atoms (Bergeron, Saumon & Wesemael 1995; Hansen 1998; Saumon & Jacobson 1999; Borysow & Jørgensen 2000). For non-polar molecules, collision-induced absorption may be-

come the dominant source of opacity over a wide range of the infrared part of the spectrum. Hydrogen and helium are the most abundant atoms in stellar atmospheres but helium does not form molecules and H_2 is non-polar; therefore, both collision-induced absorption involving H and He ($H_2 - H_2$ and $H_2 - He$), and molecules composed of less abundant elements (C, N, O, Ti, and others), if present, dominate the opacity in cool stars.

On the other hand, it is well known (e.g. Hurley & Shara 2003; Bedin et al. 2005, 2010; Salaris et al. 2010), that the blue hook seen in white dwarf cooling sequences of clusters is mainly caused by a spread in mass. In a star cluster, the massive white dwarf stars form first from the most massive progenitors and, as time goes by, the less massive white dwarf stars only get to the top of the cooling sequence. Also, the more massive the white dwarf star is, the smaller it is and the slower it cools - until crystallisation. So, in a star cluster, as the star evolves, the white dwarf cooling sequence becomes redder in the colour-magnitude diagram, and the less massive white dwarf stars reach the luminosity of the more massive ones, causing the blue turn at the bottom of the cooling sequence.

With HST photometry, Bedin et al. (2005, 2008a,b, 2010, 2015) reached the end of the white dwarf cooling sequence of the open clusters NGC 6791, NGC 2158 and NGC 6819, that also presented the blue turn feature. For NGC 6791, they determined a discrepancy between the age from the white dwarf stars (6 Gyr) and that from the main sequence turnoff (8 Gyr). García-Berro et al. (2010) argued that, if only the carbon-oxygen phase separation is taken into account, the age of NGC 6791, determined by white dwarf cooling sequence would increase to only 6.4 ± 0.2 Gyr, in disagreement with the age determinations by the main sequence turn-off (8 – 9 Gyr, Bedin et al. 2005). But, if they considered a combination of ^{22}Ne sedimentation and carbon-oxygen phase separation (Deloye & Bildsten 2002; Bedin et al. 2008a,b), the white dwarf age corresponded to 8.0 ± 0.2 Gyr (García-Berro et al. 2010). They also argued that the blue turn in the white dwarf cooling sequence is caused by the most massive white dwarf stars of the cluster, in agreement with Hurley & Shara (2003).

The blue turn feature observed in NGC 6397, and also detected in the globular clusters M 4 and 47 Tuc (Bedin et al. 2009; Kalirai et al. 2012), has been discussed by Hansen et al. (2007); Richer et al. (2013), in terms of collision induced absorption, instead of a mass effect.

The truncation of the white dwarf cooling sequence is a very sensitive age indicator as it is the limit at which most white dwarfs can have cooled in the lifetime of a cluster (Bedin et al. 2009), demanding an accurate description of this feature in order to obtain precise determinations of the ages of the clusters through the white dwarf cooling sequence.

Our main goal is to investigate the white dwarf cooling sequences of globular clusters. We use our isochrone models of the white dwarf cooling sequences calculated with metallicities consistent with the ones from each cluster and fix the initial-to-final mass function to the metallicity dependent ones from Romero, Campos & Kepler (2015). Thus, we determine the distance modulus, reddening, age and the parameter α from the present day local mass function for NGC 6397 and 47 Tuc.

This paper is organised as follows: in Sect. 2 we give a brief description of the photometric data used in our paper. In Sect. 3 we describe the evolutionary models and the white dwarf cooling sequences we used to build our white dwarf isochrones. In Sect. 4 we show our analysis and in Sect. 5 we discuss the results obtained. Concluding remarks are given in Sect. 6.

2 DATA

We perform our analysis based on the photometric data of the white dwarf stars belonging to the globular clusters NGC 6397, 47 Tucanae and M 4 (Fig. 1), obtained with the *Advanced Camera for Surveys* (ACS) of the *Hubble Space Telescope* (*HST*). These clusters are the only globulars to date with available data reaching the red end of the white dwarf cooling sequence, showing the turn towards bluer colours for the coolest white dwarf stars.

2.1 NGC 6397

The deep photometry of NGC 6397 was obtained by Richer et al. (2006) as part of a large observation program in *HST* Cycle 13 (GO-10424, PI: H. Richer) totalling 126 orbits. The data consists of 252 exposures (179.7 ks) in the F814W filter and 126 exposures (93.4 ks) in F606W. After they obtained the photometry, Richer et al. (2006) applied image spread tests to determine which sources were stellar (star-galaxy separation). To obtain the proper motion cleaned colour-magnitude diagram, Richer et al. (2006) determined the displacements between the 2005 ACS data and the WFPC2 images taken in 1994 and 1997, centred at the same coordinates, with respect to member stars, and with this, the zero point of motion of the cluster. All stars lying below the 2σ error box in the proper motion distribution in each magnitude were considered cluster members (Anderson et al. 2008).

2.2 47 Tucanae

For 47 Tuc our analysis was based on the photometric data obtained with 121 orbits in *HST* Cycle 17 (GO-11677, PI: H. Richer). Kalirai et al. (2012) describe the observations as 117 long exposures in F606W (163.7 ks) and 125 in F814W (172.8 ks). The observations were centred at about 6.7 arcmin west of the cluster centre which had previous data observed with ACS, making it possible to obtain the proper motion separation, in a similar way to the study made by Anderson et al. (2008) for NGC 6397.

2.3 M 4

Bedin et al. (2009) were able to reach the end of the white dwarf cooling sequence, at $m_{F606W} = 28.5 \pm 0.1$, with 14 *HST* orbits. The M 4 data was obtained in different programs, consisting of 20 exposures in the F606W filter (10 orbits) and 4 exposures in F775W (2 *HST* orbits) as part of the program GO-10146 (PI: L. Bedin) in *HST* Cycle 13, and F775W filter data from *HST* Cycle 11 (GO-9578, PI: J. Rhodes), consisting of 10 exposures of 360 s (2 *HST* orbits). The program GO-10146 also obtained short exposures

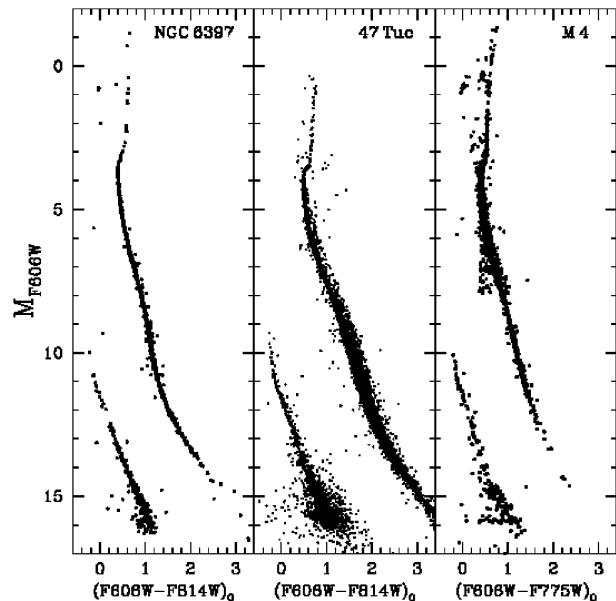


Figure 1. Proper motion cleaned colour-magnitude diagrams NGC 6397, 47 Tuc and M 4. The axes in this plot are absolute magnitude and intrinsic colour in F606W. The data in this plot has proper motion correction for all clusters. Apparent distance modulus and reddening applied for the clusters are those from Richer et al. (2013) and references therein.

in both F606W and F814W filters, and F606W archival material from program GO-10775 (PI: Sarajedini). Proper motions were measured with a technique similar to that described in Bedin et al. (2003, 2006), also considering the zero point of the motion of the cluster.

3 EVOLUTIONARY MODELS

White dwarf evolutionary models used in our analysis are those computed by Romero, Campos & Kepler (2015) for different metallicities. These models are the result of computations employing the LPCODE evolutionary code, the same code used by Althaus et al. (2005, 2015) and Renedo et al. (2010). They computed the evolution from the Zero Age Main Sequence, through the hydrogen and helium central burning stages, the full thermally pulsing and mass loss stages on the Asymptotic Giant Branch, and finally through the white dwarf cooling curve.

The models also incorporate the effects of possible residual hydrogen burning present in low-metallicity progenitors, for which the mass loss is less efficient and as a result, the thickness of the hydrogen layer left on the white dwarf model increases with decreasing metallicity. Then, the larger the hydrogen mass on the envelope of the white dwarf the more efficient the residual burning at high effective temperatures on the cooling sequence (Renedo et al. 2010; Miller Bertolami et al. 2013).

Here, we briefly mention some of the main input physics relevant for this work. A detailed description can be found in Althaus et al. (2005) and Romero, Campos & Kepler (2015). During the white dwarf cooling, the code considers

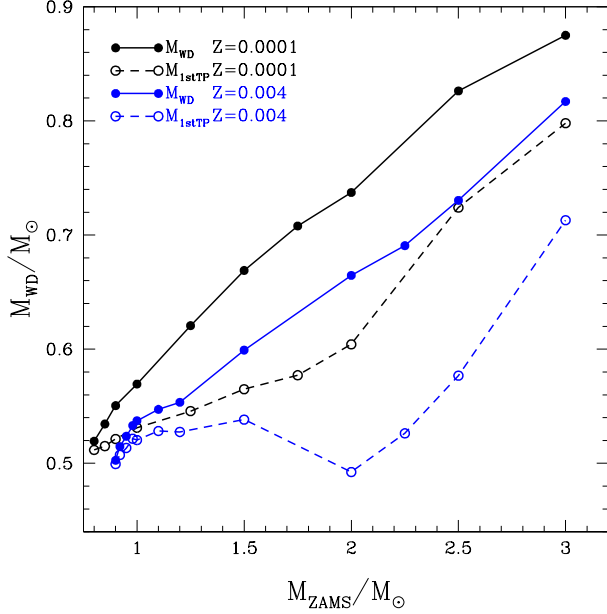


Figure 2. Initial - Final mass relation from Romero, Campos & Kepler (2015) considering the final mass as the mass of the hydrogen free core at the first thermal pulse (hollow circles) and as the mass of the white dwarf at the cooling curve (full circles). Black and blue curves correspond to sequences with initial metallicity $Z=0.0001$ and $Z=0.004$, respectively.

element diffusion due to gravitational settling, chemical and thermal diffusion (Althaus et al. 2003). At effective temperatures below 10 000 K on the cooling curve, the outer boundary conditions are derived from non-grey atmosphere models from Rohrmann et al. (2012) which include the tail of Ly α in the optical (Kowalski 2007). The release of latent heat and gravitational energy due to carbon-oxygen phase separation is included following the Horowitz, Schneider & Berry (2010) phase diagram, consistent with the observations by Winget et al. (2009, 2010) and the massive pulsating white dwarf stars studied in Romero et al. (2013).

We consider main sequence masses from ~ 0.8 to $\sim 6.0 M_{\odot}$, where the low mass limit depends on metallicity. The resulting white dwarf models show stellar mass values from ~ 0.50 to $\sim 1.00 M_{\odot}$. Note that this mass interval corresponds to carbon-oxygen core stars. We consider the mass of the white dwarf as the actual final mass in the cooling curve, not the approximation of the mass of the hydrogen free core at the first thermal pulse. At the end of the AGB stage, when the star becomes a thermally pulsing TP-AGB star, the mass of the hydrogen free core will increase with each thermal pulse. Kalirai, Marigo & Tremblay (2014) estimated a growth of the core mass between 10% to 30% for a progenitor of 1.6 - $2.0 M_{\odot}$. Therefore the mass at the cooling curve is larger than the core mass at the first thermal pulse, leading to a different initial-to-final mass prescription. Figure 2 shows the initial-to-final mass relation resulting from Romero, Campos & Kepler (2015) computations for $Z=0.0001$ and $Z=0.004$. With filled circles we depict the initial-to-final mass with a white dwarf mass correspond to the mass of the model at the cooling curve, while hol-

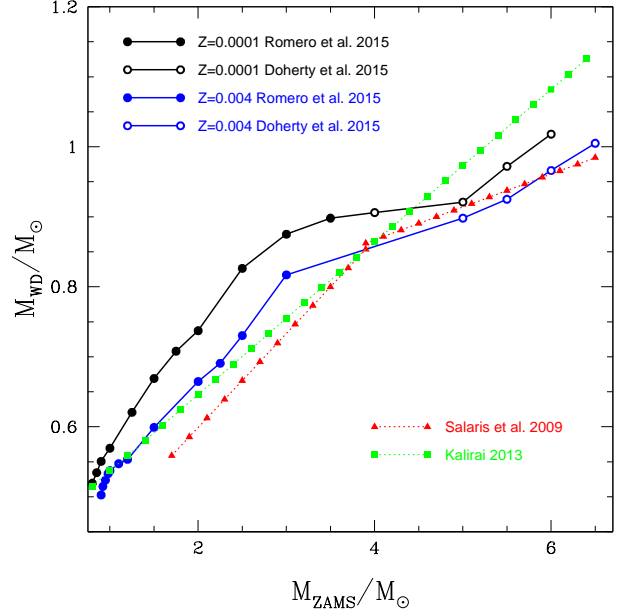


Figure 3. Initial - Final mass relation from Romero, Campos & Kepler (2015) (filled circles) and Doherty et al. (2015) (hollow circles) for the metallicities of $Z = 0.0001$ and $Z = 0.004$ and. The range of progenitor masses are $0.8 - 3.0 M_{\odot}$ for Romero, Campos & Kepler (2015) models and ~ 4.0 - $7.0 M_{\odot}$ for Doherty et al. (2015) models. The red triangles and green squares represent the semi-empirical initial-to-final mass from Salaris et al. (2009) and Kalirai (2013) that do not take different metallicities into account.

low circles shows the mass of the hydrogen free core at the first thermal pulse. At the low mass end, the increase of the core mass during the TP-AGB is small, because of the small number of thermal pulses. However, as the initial mass increases, the number of thermal pulses also increases and so will the mass of the hydrogen free core.

Romero, Campos & Kepler (2015) compare their results with those obtained by other authors. They found that, at the low mass end the initial-to-final mass agrees with that of Weiss & Ferguson (2009), especially for high metallicity progenitors, while for high masses and low metallicities the differences became more important. The white dwarf masses from Weiss & Ferguson (2009) are smaller than those from Romero, Campos & Kepler (2015), because Weiss & Ferguson (2009) calculations allow overshooting during the TP-AGB, limiting the growth of the hydrogen-free core. In fact, the initial-to-final mass of Romero, Campos & Kepler (2015) for the core mass at the first thermal pulse. Note that pre-white dwarf ages for high mass progenitors, where the effects of overshooting during the TP-AGB are more important, do not change considerably with initial mass (see Tab. 1 from Romero, Campos & Kepler (2015)).

Romero, Campos & Kepler (2015) also compared sequences with initial mass $1 M_{\odot}$ and metallicity of $Z=0.0001$ and $Z=0.02$ using MESA (Paxton et al. 2011, 2013) including similar mass loss. As a result, they found that LPCODE lifetimes were consistent with those computed with MESA,

resulting in differences smaller than ~ 0.1 Myr at $\sim 25\,000$ K on the white dwarf cooling curve.

In order to extend our mass range, we included additional white dwarf sequences with stellar masses up to $\sim 1.0M_{\odot}$, corresponding to progenitor masses up to $6M_{\odot}$ for $Z = 0.0001$ and $7M_{\odot}$ for $Z = 0.004$. We adopt the initial-to-final mass from Doherty et al. (2015) for carbon-oxygen white dwarf remnants with the metallicities of $Z = 0.0001$ and $Z = 0.004$. To compute the white dwarf evolution, we took a white dwarf model at high effective temperatures at the beginning of the cooling curve for the highest stellar mass evolutionary model available in our original grid, and artificially scaled the stellar mass from Romero et al. (2013). We also changed the carbon/oxygen central composition to match that from Doherty et al. (2015) for each stellar mass and metallicity. The pre-WD ages were taken from Doherty et al. (2015) computations. Further evolution on the white dwarf cooling sequence was computed employing the LPCODE, including all physical ingredients considered in white dwarf computations from full evolution. Figure 3 shows the initial-to-final mass extended to progenitor masses of $\sim 7M_{\odot}$. Filled circles corresponds to full evolutionary computations (same as figure 2) while hollow circles correspond to Doherty et al. (2015) results. We also compare with the semi-empirical initial-to-final mass from Salaris et al. (2009) and Kalirai (2013). Note that semi-empirical determinations of the initial-to-final mass relations do not take different metallicities into account.

We use the colours of the white dwarf cooling models consistent with those from recent results by Tremblay et al. (2010) that include the Lyman- α red wing calculations from Kowalski & Saumon (2006). The HeH^+ molecule in the equation of state, which becomes very important at $T_{\text{eff}} < 8000$ K, is also included (Harris et al. 2004; Kilic et al. 2010).

We also explored the possibility of white dwarf atmospheric models composed by a mixture of hydrogen and helium. The colours of the atmosphere models with hydrogen and helium mixed consider thick hydrogen layers ($q_H \equiv M_H/M_{\star} = 10^{-4}$) for low He/H ($\text{He}/\text{H} \leq 1$). For higher He/H values, thin hydrogen layers ($q_H \equiv 10^{-10}$) were considered. Those models were calculated ranging from $\log(\text{He}/\text{H}) = -2$ to $\log(\text{He}/\text{H}) = 8$.

4 DATA ANALYSIS

Richer et al. (2013) argued that the difficulty in age determination through the main sequence turn-off lies in the fact that the differences between two or more clusters can be due to metallicity and/or age differences. They compared the white dwarf cooling sequences of 47 Tuc, NGC 6397 and M4, considering the properties, distance modulus and reddening. They demonstrated that the white dwarf cooling sequences of those three clusters almost align perfectly in the colour-magnitude diagram, as seen in Fig. 1, even though they have different metallicities. This is consistent with the timescales of diffusion processes in the white dwarf atmospheres (Fontaine & Michaud 1979). Richer et al. (2013) claimed that white dwarf spectra and location on the colour-magnitude diagram do not depend on the cluster metal abundance, unless there is a possible dependence of the

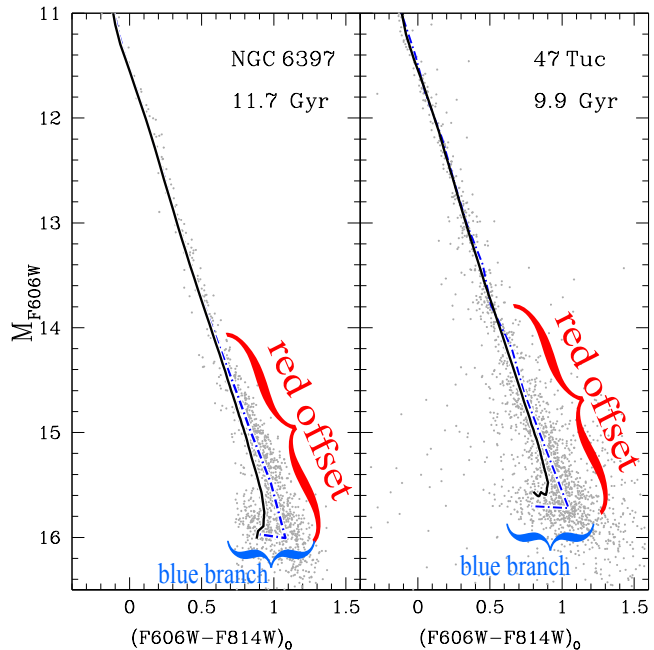


Figure 4. Our isochrone models (solid black line), with the ages determined by Hansen et al. (2013) over-plotted to the white dwarf cooling sequences of NGC6397 and 47Tuc. The blue dot-dashed line represents a mean ridge line of the data. The distance modulus and reddening correction are the ones by Richer et al. (2013). For 47 Tuc, the “blue branch” of the isochrone with 9.9 Gyr model happens at a magnitude brighter than the one from the data. The red offset feature is also highlighted in the colour-magnitude diagram of both clusters.

white dwarf mass on metallicity through the initial-to-final mass relation (Kalirai et al. 2005, 2008, 2009).

Our first step was comparing our pure hydrogen isochrone models (Sect. 3), with the ages determined by Hansen et al. (2013), to the white dwarf cooling sequences of NGC 6397 (11.7 Gyr) and 47 Tuc (9.9 Gyr). In Fig. 4 we can see that, especially for 47 Tuc, the “blue branch” of the model happens at a brighter magnitude than the one from the data. Also, if we compare the mean ridge line of the data (blue dot-dashed line) to the isochrone models, for both clusters, Fig. 4 also highlights a change in the slope of the white dwarf cooling sequence after $F606W \sim 14.5$, showing a trend for the models to be bluer (brighter) than the data, that is, a red offset of the data.

Such trend could be caused by problems in the photometric calibration, so, before we began our analysis, we calculated the mean ridge line of the Small Magellanic Cloud (SMC) that is present in the non proper motion-corrected data of 47 Tuc (e.g. Kalirai et al. 2012; Richer et al. 2013), in an attempt to test this hypothesis. The mean ridge line of the SMC does not present the same trend towards redder colours as the one from the white dwarf cooling sequence of 47 Tuc, indicating that poor photometric calibration is, apparently, not causing this slope change.

This mismatch between models and data in the white dwarf cooling sequence is in the same line of problems found in the comparison of main sequence models to the data. For example, Chen et al. (2014) has shown that for low mass main sequence stars – the coolest stars in the main sequence

– the data is redder than the models, even after they adopt better bolometric correction tables and new $T - \tau$ relations. They also mention that this problem seems to extend to other sets of models in the literature.

Clearly, there are aspects of the construction of the models of white dwarf stars that need further investigation. We estimate that $\sim 19\%$ of the total number of observed white dwarf stars lie on the red offset portion. One possible explanation for the red offset of the white dwarf stars could be a fraction of pure helium atmosphere white dwarf stars that would move the models to bluer colours. White dwarf masses would have to be $\sim 0.55 M_{\odot}$ at the bottom of the cooling sequence for the models to deviate as much as the data.

Hansen et al. (2004) and Bedin et al. (2009) included the fraction of helium atmosphere in their analysis of the white dwarf population of M4. Hansen et al. (2004) treated it as a free parameter and estimated an upper limit of 40%, while Bedin et al. (2009) fixed the fraction at 30%, the typical value for the DB/DA ratio in the disk population. However, Davis et al. (2009) analysed the spectra of 24 bright white dwarf stars in the line of sight of M4 and determined that all had hydrogen atmospheres. They argued that if all the 24 white dwarf stars were members of the cluster, the probability of observing helium atmosphere white dwarf stars is 6×10^{-3} . Davis et al. (2009) thoroughly discussed the probability of finding helium atmosphere white dwarf stars in globular clusters, including results from other authors. They concluded that it is clear that the hydrogen/helium white dwarf stars atmosphere ratio in globular clusters is lower than in the field and that even though it is not impossible to form a non-hydrogen atmosphere in the cluster environment, the formation mechanism is clearly strongly suppressed. So, it is very unlikely that a fraction of 30 to 40% of helium atmosphere white dwarf stars are observed in globular clusters.

Davis et al. (2009) only used the spectra of hot white dwarf stars in globular clusters. However, there is little spectra information on white dwarf stars with effective temperatures lower than ~ 5000 K. Limoges, Bergeron & Lépine (2015) performed a census of white dwarf stars within 40 pc of the Sun and found that probably most white dwarf stars with $T_{\text{eff}} < 5000$ K have pure hydrogen atmospheres. However, they pointed out that the results below $T_{\text{eff}} = 5000$ K should be considered with caution. Depending on the resolution, the spectra of ultra cool white dwarf stars do not show hydrogen or helium lines, thus providing no information on their surface gravities. So, inferences on the composition of the atmosphere can only be modelled with an analysis of the energy distribution (Bergeron, Saumon & Wesemael 1995).

Koester (1976), Vauclair & Reisse (1977) and D’Antona & Mazzitelli (1979) independently proposed the existence of a convective mixing between the massive helium layer and the thin hydrogen layer above it for cool white dwarf stars. When in the mixing process, the convection zone of a hydrogen atmosphere white dwarf star eventually reaches the underlying helium layer, helium will be brought to the surface through convective motion, resulting in the mixing of hydrogen and helium layers. Bergeron et al. (1990) showed that the surface gravities, inferred from spectroscopy of a sample containing 37 cool white dwarf stars ($T_{\text{eff}} \lesssim 12000$ K), were significantly

larger than the canonical value expected for these stars ($\log g \sim 8$), and that was interpreted as an evidence of the convective mixing between the hydrogen and helium layers. However, with high signal-to-noise, high-resolution spectroscopic observations for six cool DA white dwarf stars ($10720 \text{ K} \lesssim T_{\text{eff}} \lesssim 12630 \text{ K}$), obtained with the Keck I telescope, Tremblay et al. (2010) detected no helium in the spectra of any of the target stars, concluding that their helium abundance allowed to rule out the incomplete convective mixing scenario as the source of the high- $\log g$ problem. Later, Tremblay et al. (2013, 2015) found that the the imprecise convection calculation was suppressing the convective mixing scenario.

The results from Tremblay et al. (2010) do not rule out the hypothesis of mixed atmosphere for ultra-cool white dwarf stars ($T_{\text{eff}} \lesssim 5000 \text{ K}$). Calculations by Tremblay & Bergeron (2008) indicate that the effective temperature at which the mixing would occur depends on the thickness of the hydrogen envelope, meaning that, the thicker the envelope, the lower the mixing temperature. Tremblay & Bergeron (2008) showed that the mixing should not occur if the mass of the hydrogen layer is larger than $M_H/M_{\star} \sim 10^{-6}$. Chen & Hansen (2011) presented a theoretical analysis of white dwarf stars with the hydrogen layer mass between 10^{-7} and $10^{-11} M_{\star}$. They showed that a white dwarf star, upon convective mixing, always decreases the amount of hydrogen on the surface, but the spectral outcome and the change in the effective temperature depends on the mass of the hydrogen layer.

The existence of white dwarfs with the thickness of the hydrogen layer between $10^{-9.5} < M_{\star} < 10^{-4}$ was shown by Castanheira & Kepler (2008, 2009) and Romero et al. (2012, 2013), through asteroseismological studies. Castanheira & Kepler (2008) argue that this indicates that white dwarfs with an atmosphere of H, even if their total masses are close to the most probable value, may have formed with a H mass several orders of magnitude smaller than the value predicted by theory, i.e., it is likely that the mass loss during its evolution was actually more efficient than assumed by evolutionary models including mass loss of Reimers (1977), Vassiliadis & Wood (1993) and Groenewegen et al. (2009). The most probable scenario is that the star might have experienced a late thermal pulse that consumed most of its hydrogen layer leaving a very thin ($10^{-8} - 10^{-10}$) hydrogen layer.

Preliminary tests with our models show that, for the mixing of hydrogen and helium to occur at temperatures consistent with the change in slope of the models ($T_{\text{eff}} \sim 5000 \text{ K}$), the mass of the hydrogen layer should be between 10^{-6} and $10^{-7} M_{\star}$, and the atmosphere would not be turned into pure helium. Instead, the atmosphere would be composed by hydrogen with traces of helium. When this mixing occurs, the atmosphere becomes more transparent and appears slightly hotter, causing a shift to a brighter magnitude; after that, the star continues to cool, but not as a pure hydrogen atmosphere anymore. This effect could be the reason of the observed slope change of the white dwarf cooling sequence from the globular clusters; however, this requires further investigation and proper modelling of the convective processes.

Also, to perform an analysis of such cold white dwarf stars with mixed atmospheres, we should consider that, bel-

low 16 000 K, line broadening by neutral particles becomes important at helium rich atmospheres (Koester & Kepler 2015). However, only some He transitions have so-called self broadening theories, and they were tested for very low temperatures (300 K). How calculations for appropriate temperatures would affect the models is still unknown.

Assuming that mixing of hydrogen and helium occurs in the atmosphere of the very cool white dwarf stars ($T_{\text{eff}} \lesssim 6000$ K), Saumon, Holberg & Kowalski (2014) studied the near-UV absorption in white dwarf stars with models containing the revised calculations of $H_2 - He$ collision-induced absorption opacity from Abel et al. (2012). We compared our single mass white dwarf model for $0.60 M_{\odot}$ with $\log(\text{He}/\text{H})=0$ to the one by Saumon, Holberg & Kowalski (2014) with the newest opacity, with the same parameters, and we found no difference between models with the new and old $H_2 - He$ collision induced absorptions for $T_{\text{eff}} \gtrsim 5000$ K. Saumon, Holberg & Kowalski (2014) mention the fact that $H_2 - H_2$ calculations are still in progress, so if they will help to solve the red offset problem is an important open question.

4.1 Comparison of models with data

Hansen et al. (2007) pointed that an important part of modelling Monte Carlo simulations is the need to have the same observational scatter and incompleteness as the data. This is even more important for white dwarf stars, as even the brightest ones could be lost if they are close to a bright main sequence star. To take that into account, Hansen et al. (2007, 2013) performed artificial star tests so they could measure the recovery fraction and determine the association between input and observed magnitude.

To obtain the cluster parameters we used our isochrone models to generate Monte Carlo realisations of the white dwarf populations and compared them with the observed cooling sequences.

Our Monte Carlo simulations follow an inverse transform sampling (Fisherman 1996). For the mass interval represented in the observed luminosity function, we are assuming a single burst star formation and a Salpeter (1955) distribution ($dN/dM \propto M^{-\alpha}$) for the present day local mass function. We allowed α to vary from 1.6 to 4.0. As we are not considering any dynamical effects in our models, we are only obtaining the present day local mass function. As the mass of the progenitor star represented in the observed luminosity function from the white dwarf stars is only from 0.85 to ~ 6.00 , we assumed a single burst star formation. We also adopt the metallicity dependent initial-to-final mass relation from Romero, Campos & Kepler (2015) and generate models with a range of distance modulus and reddening appropriate to each cluster.

To account for the size of the photometric errors, for each model white dwarf star we add a photometric uncertainty that was determined through artificial star tests consistent with NGC 6397 and 47 Tuc (Hansen et al. 2007, 2013). The artificial star tests provide not only the degree of correlation between the input and observed magnitudes, but also the recovery fraction, i.e., the photometric completeness of the data, which is also taken into account in our simulations. This process was applied for both F606W and F814W filters. Thus, each realisation includes realistic photometric

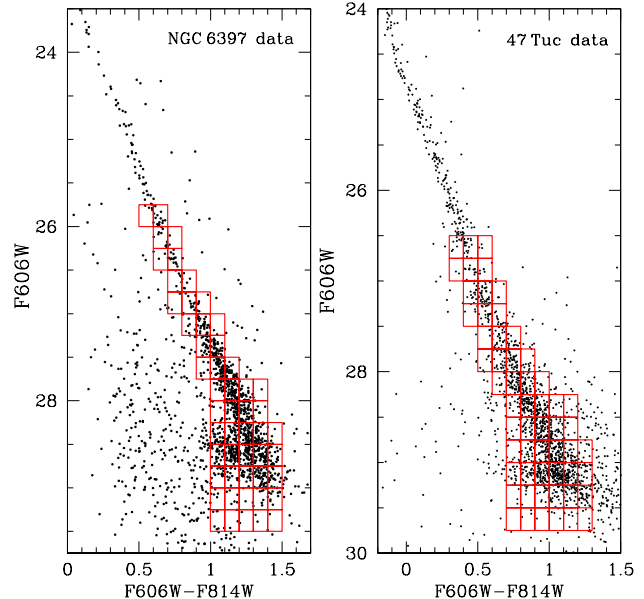


Figure 5. The red grid overlaid on the white dwarf cooling sequences of NGC 6397 and 47 Tuc illustrating the way the data were binned in order to compare the observations to the Monte Carlo simulations with Hess diagrams. Each bin measures 0.25 mag in magnitude and 0.1 mag in colour.

scatter and the correct level of completeness. Our Monte Carlo simulations do not account for the effect of multiple star formation bursts, unresolved binaries or multiple populations.

To reduce model uncertainties we generated simulations with 20 000 stars. Observed and model luminosity functions are built with bins of 0.20 mag; Hess diagrams are binned with a grid width of 0.1 mag in F606W-F814W and 0.25 mag in F606W, a grid similar to that used in previous analysis of the same data (Hansen et al. 2007, 2013; García-Berro et al. 2014; Torres et al. 2015), as shown in Fig. 5. Simulations are normalised to have the same number of stars as the corresponding cluster.

To compare the Hess diagrams of the models and the observations we used the reduced χ^2_{red} which is the sum of the residuals taking the density of the observed and model of each grid cell into account, according to:

$$\chi^2 = \sum_i \frac{(O_i - E_i)^2}{\sigma_{O_i}^2} \quad (1)$$

where E_i is the number of events expected according to the model O_i is the number observed in the i th bin and, as we assume our data follow a Poisson distribution, σ_{O_i} is the uncertainty in the number of observed stars ($\sqrt{O_i}$).

We compute independent χ^2 tests for the luminosity function and for the Hess diagram. The χ^2 tests for the colour functions is not computed because the red offset masks the information. After that we obtained the reduced χ^2 for both approaches. Hereafter, we followed the process adopted by García-Berro et al. (2014) and Torres et al. (2015), and the reduced χ^2 values were normalised to the minimum value for each of the tests and added quadratically. Torres et al. (2015) argued that although they have used a

χ^2 test, their final aim was to estimate the values of the free parameters that best fit the observed data, rather than obtaining an absolute probability of agreement of the models with the observed data. That is precisely the same goal we have in our analysis, therefore using the same kind of analysis employed by García-Berro et al. (2014) and Torres et al. (2015) is a meaningful approach.

To begin our analysis we obtained the distance modulus and reddening from the data by comparing the Monte Carlo simulations to the data of the white dwarf stars hotter than ~ 5500 K, i.e., the top of the white dwarf cooling sequence. Also, we compare our age and α determinations to the ones found if we fix the distance modulus and the reddening obtained through isochrone fittings to the main sequence for NGC 6397 ($\mu_0=12.07\pm0.06$ and $A_V=0.56\pm0.06$, Richer et al. 2008) and 47 Tuc ($\mu_0=13.26$ and $A_V=0.07$, Dotter et al. 2010).

The results from our analysis for NGC 6397 and 47 Tuc, performed as explained above, are shown in Sect. 4.1.1 and 4.1.2.

4.1.1 NGC 6397

The fitting of the white dwarf stars hotter than 5000 K to our Monte Carlo simulations resulted in a distance modulus of $\mu_0=11.85\pm0.04$ and $A_V=0.64\pm0.04$, or $E(B-V)=0.21$ (assuming $R_V = 3.1$). These values are in agreement, within the uncertainties, with the ones presented by Richer et al. (2013) and references therein.

After that we performed the fitting of our Monte Carlo simulations to the data allowing age and α to vary and keeping the distance modulus and reddening as fixed parameters. The range of ages for NGC 6397 was set to vary from 12.0 to 13.3 Gyrs and α , of the present day local mass function, could vary from 3.0 to 1.6. The χ^2 is presented in Fig. 6, we also show the curves enclosing the regions with 68%, 95% and 99% confidence level using lines. The model that best fit the data has an age of $12.93^{+0.37}_{-0.21}$ Gyr and $\alpha=2.17^{+0.34}_{-0.30}$ is marked as a white cross.

We also tested fixing the distance modulus and the reddening to the ones by Richer et al. (2008), obtained by fitting models to the main sequence of NGC 6397 data obtained with Hubble Space Telescope, $\mu_0=12.07\pm0.06$ and $A_V=0.56\pm0.06$. In that way we test the effect of keeping the coherence between the main sequence and the white dwarf cooling sequence. The results for the χ^2 is presented in Fig. 7. The model that we found as the one that best fitted the data in this case has an age of $12.48^{+0.39}_{-0.26}$ Gyr and $\alpha=2.31^{+0.39}_{-0.33}$.

When we compared the age and α obtained with our distance modulus and reddening to the results obtained with the distance modulus and reddening consistent to the main sequence by Richer et al. (2008) we obtain differences of 0.45 Gyrs in age and 0.14 in α . Both determinations are consistent, within the uncertainties, and the age difference is smaller than the uncertainties of our models of the order of 0.50 Gyrs.

Figure 8 shows the luminosity function of our best fit Monte Carlo simulations compared to the data. As our simulations have 20 000 stars, we normalised the simulations to the total area of the data. At the top panel we show the best fit model obtained with our distance modulus and

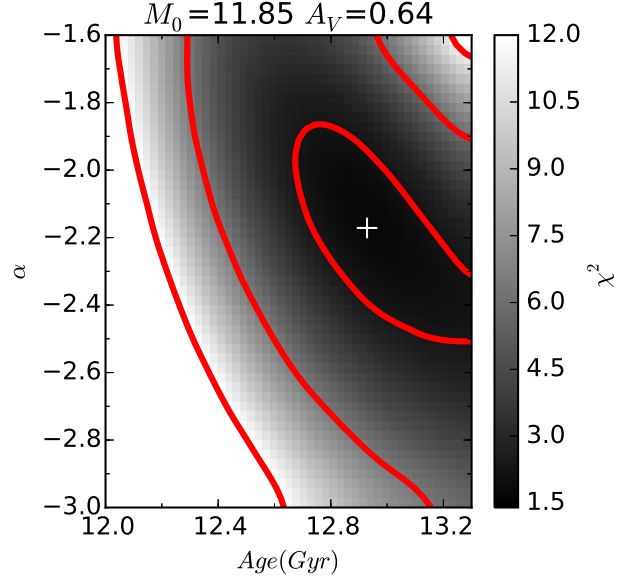


Figure 6. χ^2 (grey scale) for age and α for NGC 6397 with our determination of distance modulus and reddening considering only the white dwarf stars hotter than 5000 K. The red lines represent the regions with 68%, 95% and 99% confidence level and the white cross represents the best fit model.

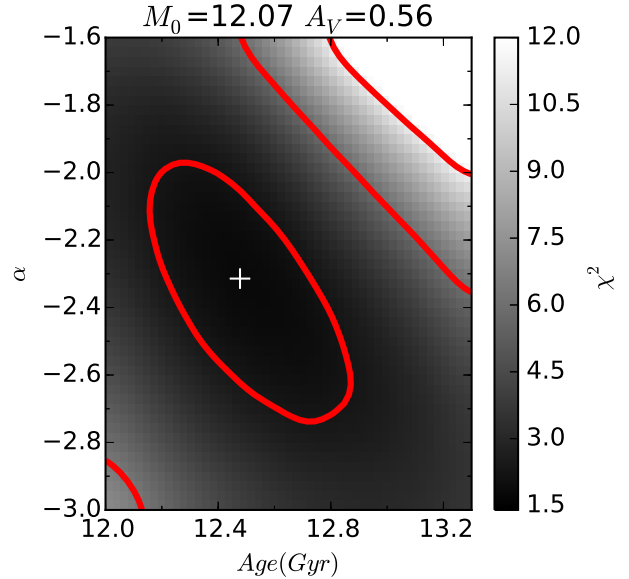


Figure 7. χ^2 (grey scale) for age and α for NGC 6397 with the determination of distance modulus and reddening obtained by Richer et al. (2008) through the main sequence fitting. The red lines represent the regions with 68%, 95% and 99% confidence level and the white cross represents the best fit model.

reddening determination. In the lower panel we show the luminosity function of our model with the distance modulus and reddening obtained by Richer et al. (2008).

It is clear, from Fig. 8, that the model with our distance modulus and reddening determinations presents a better fit to the data, mainly for the fainter white dwarf stars. However, for the brightest white dwarf stars, both models present

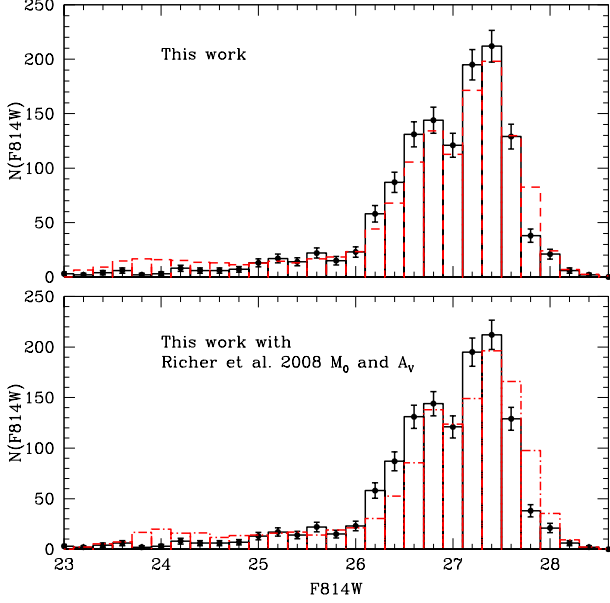


Figure 8. Luminosity function of NGC 6397 (solid black line) compared to the best fit models. At the top panel we show the model with $12.93^{+0.37}_{-0.21}$ Gyr and $\alpha=2.17^{+0.34}_{-0.30}$, obtained with our distance modulus and reddening determination (dashed red line). While in the lower panel we show the luminosity function of our model with the distance modulus and reddening obtained by Richer et al. (2008) with $12.48^{+0.34}_{-0.26}$ Gyr and $\alpha=2.31^{+0.39}_{-0.33}$ (dot-dashed red line). The error bars are Poisson errors.

a number of stars that is higher than the one observed in the data.

We also compared our simulated luminosity function to the ones from Torres et al. (2015) and Hansen et al. (2007). In figs. 9 and 10 we show, in the top panel, the luminosity function of our best fit model compared to the data. In the lower panel of Fig. 9 we show the luminosity function of the best fit model by Torres et al. (2015) presented in their Fig. 1, compared to the data, while in the lower panel of Fig. 10 we show the luminosity function of the best fit model by Hansen et al. (2007) presented in their Fig. 15. Both Torres et al. (2015) and Hansen et al. (2007) simulations present a better fit for the hot white dwarf stars than our models with more free parameters. However, the crystallisation peak at $F814W \sim 26.8$ is not present in Torres et al. (2015) and Torres et al. (2015) simulations. Our simulation clearly presents a peak at the same magnitude as the crystallisation peak, demonstrating the quality of our models.

The comparison between the white dwarf cooling data and the Monte Carlo model that best fits the data presents an excellent agreement, as can be seen in Fig. 11, for NGC 6397. We also illustrate the spread in mass (red labels), according to the models, ranging from $\sim 0.525 M_{\odot}$, at the top of the cooling sequence, which is consistent with spectroscopic results, to $\sim 0.875 M_{\odot}$ at the bottom.

The turn to the blue is better reproduced in our models, if we compare to the one presented by Hansen et al. (2007), in their Fig. 11, where the models did not fully reproduced the clump of stars blueward of the faint end of cooling sequence and the most massive white dwarf star in

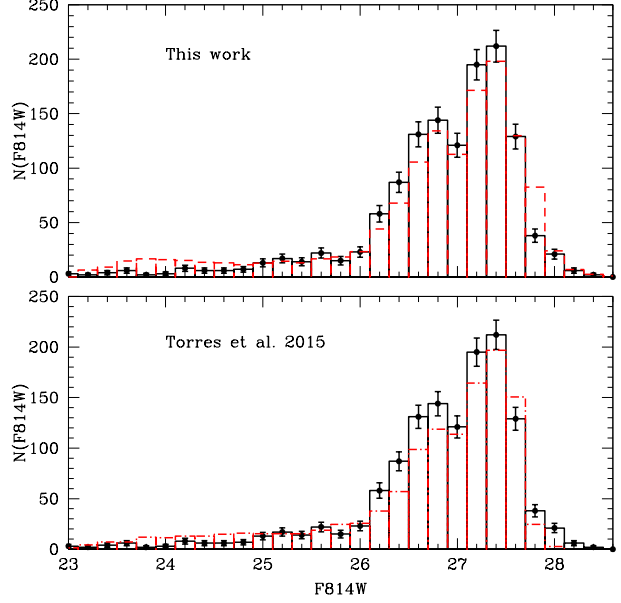


Figure 9. In the top panel, the normalised luminosity function of our best fit model (dashed red line) compared to the data of NGC 6397 (solid black line). In the lower panel we show the luminosity function presented in Fig. 1 of Torres et al. (2015) compared to the same data (dot-dashed red line). The error bars are Poisson errors.

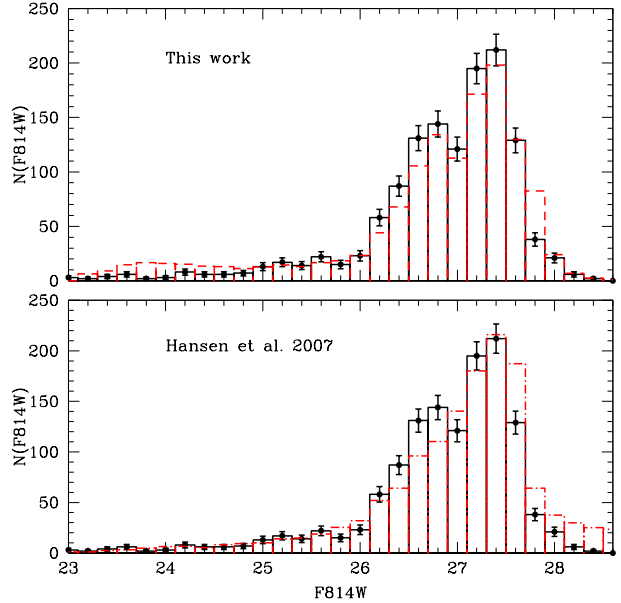


Figure 10. In the top panel, the normalised luminosity function of our best fit model (dashed red line) compared to the data of NGC 6397 (solid black line). In the lower panel we show the luminosity function presented in Fig. 15 of Hansen et al. (2007) compared to the same data (dot-dashed red line). The error bars are Poisson errors.

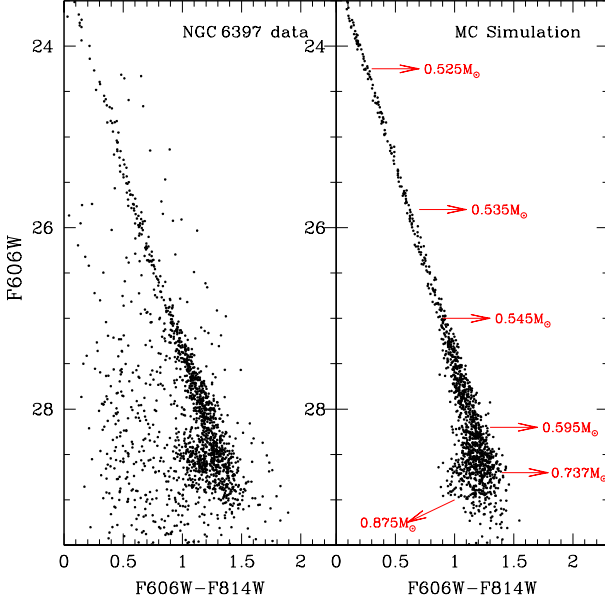


Figure 11. The left panel shows the observed white dwarf cooling sequence of NGC 6397, after the star-galaxy separation described in Hansen et al. (2007). The right panel shows the Monte Carlo simulation with 12.93 Gyr, that best fitted the data with our distance modulus and reddening determination. The red labels illustrate the spread in mass, according to the models, ranging from $0.525 M_{\odot}$, at the top of the cooling sequence, which is consistent with spectroscopic results, to $0.875 M_{\odot}$ at the bottom.

their model was $\sim 0.62 M_{\odot}$. When compared to the models by Torres et al. (2015), our colour magnitude diagram is just as good but, as discussed previously, our luminosity functions present features consistent with the data that are not apparent in Torres et al. (2015) simulations.

4.1.2 47 Tuc

By performing the fitting of the white dwarf stars hotter than 5000 K of 47 Tuc to our models we obtained the distance modulus of $\mu_0 = 13.28^{+0.06}_{-0.03}$ and $A_V = 0.14 \pm 0.01$, or $E(B-V) = 0.045$. These values are in agreement with the ones presented by Richer et al. (2013) and references therein.

So we performed the fitting of our Monte Carlo simulations to the data allowing age and α to vary and keeping the distance modulus and reddening as fixed parameters. The range of ages for 47 Tuc was set to vary from 10.2 to 12.8 Gyr and α , of the present day local mass function, could vary from 4.2 to 1.6. The χ^2 is presented in Fig. 12. The model that best fit the data has an age of $10.95^{+0.21}_{-0.15}$ Gyr and $\alpha = 3.42^{+0.50}_{-0.46}$ is marked as a white cross.

Again, to keep the coherence between the main sequence and the white dwarf cooling sequence, we fixed the distance modulus and the reddening to the ones by Dotter et al. (2010), obtained by fitting models to the main sequence of 47 Tuc data obtained with Hubble Space Telescope, $\mu_0 = 13.26$ and $A_V = 0.07$. The results for the χ^2 is presented in Fig. 13. The model that we found as the one that best fitted the data in this case has an age of $11.31^{+0.36}_{-0.17}$ Gyr and $\alpha = 3.26^{+0.53}_{-0.44}$.

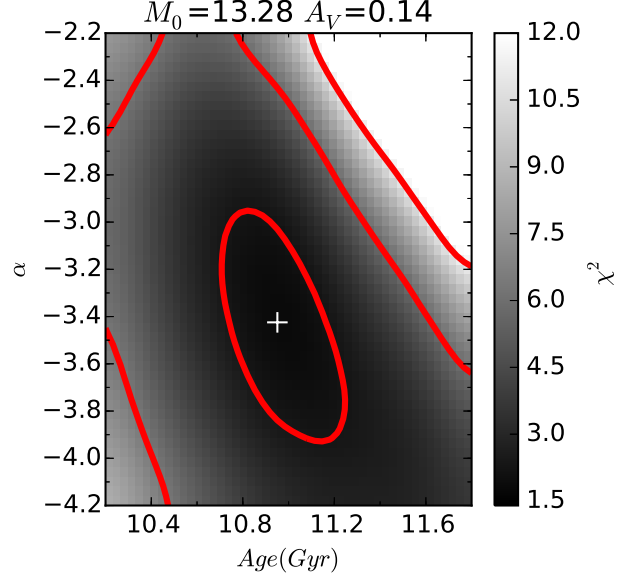


Figure 12. χ^2 (grey scale) for age and α for 47 Tuc with our determination of distance modulus and reddening considering only the white dwarf stars hotter than 5000 K. The red lines represent the regions with 68%, 95% and 99% confidence level and the white cross represents the best fit model.

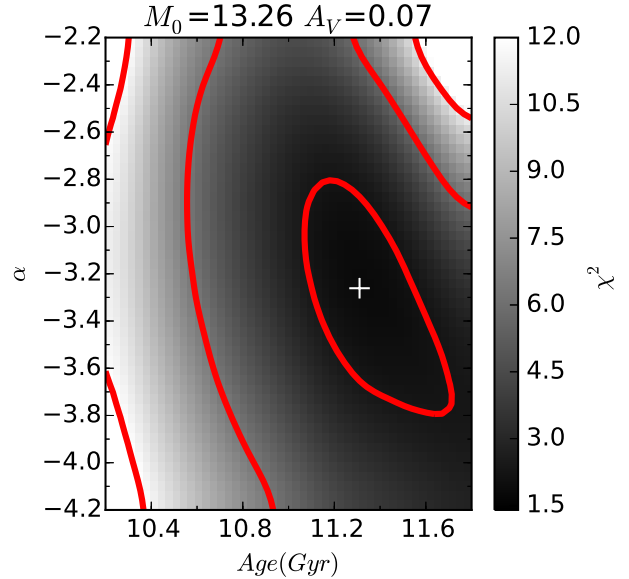


Figure 13. χ^2 (grey scale) for age and α for 47 Tuc with the determination of distance modulus and reddening obtained by Dotter et al. (2010) through the main sequence fitting. The red lines represent the regions with 68%, 95% and 99% confidence level and the white cross represents the best fit model.

Comparing the results obtained with our distance modulus and reddening to the results obtained with the distance modulus and reddening consistent to the main sequence by Dotter et al. (2010) we notice difference of 0.36 Gyr in age and 0.16 in α . Such differences in age are smaller than the uncertainties of our models of the order of 0.50 Gyr.

As Hansen et al. (2013) did not show their luminosity

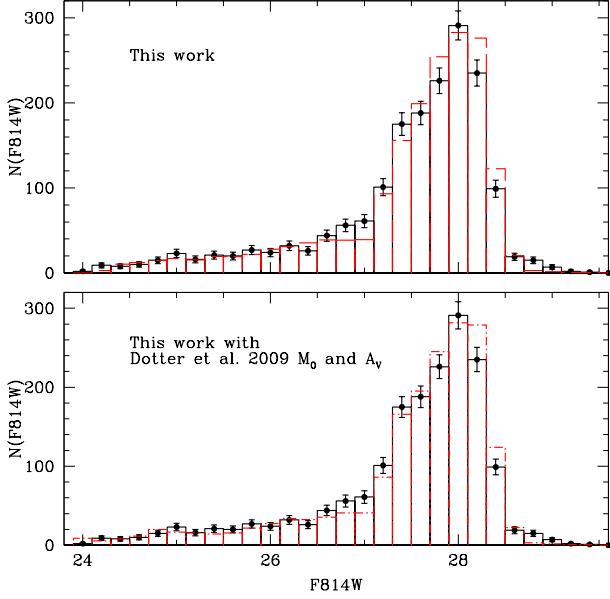


Figure 14. The normalised luminosity function of 47 Tuc (solid black lines) compared to the best fit models. At the top panel we show the model with $10.95^{+0.24}_{-0.15}$ Gyr and $\alpha=3.42^{+0.50}_{-0.46}$, obtained with our distance modulus and reddening determination (dashed red lines). While in the lower panel we show the luminosity function of our model with the distance modulus and reddening obtained by Dotter et al. (2010) with $11.31^{+0.17}_{-0.36}$ Gyr and $\alpha=3.26^{+0.53}_{-0.44}$ (dot-dashed red lines). The error bars are Poisson errors.

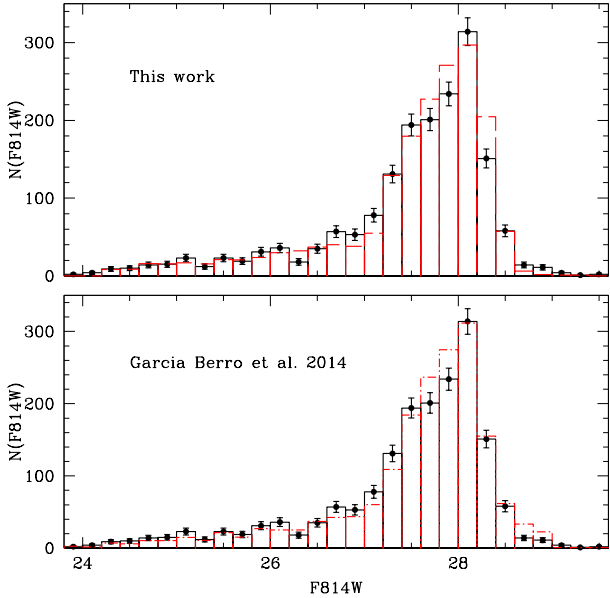


Figure 15. In the top panel, the normalised luminosity function of our best fit model (dashed red lines) compared to the data of 47 Tuc (solid black lines). In the lower panel we show the luminosity function presented in Fig. 4 of García-Berro et al. (2014), normalised to the total number of stars in our data (dot-dashed red lines), compared to the same data. The error bars are Poisson errors.

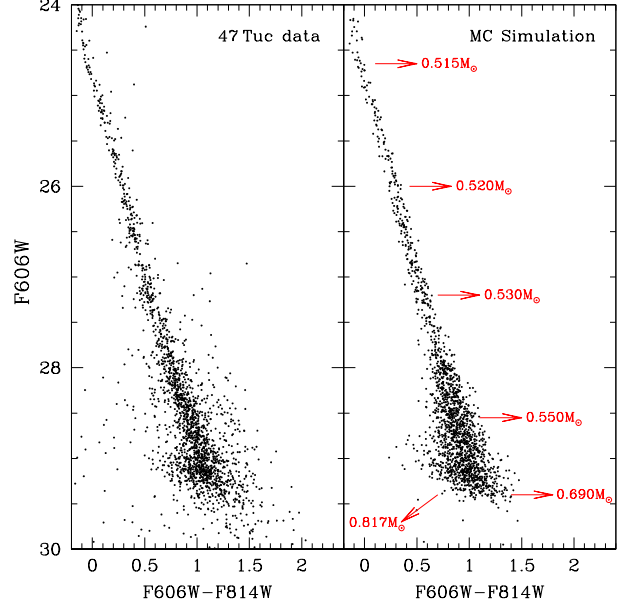


Figure 16. The left panel shows the observed white dwarf cooling sequence of 47 Tuc with the proper motion selected stars. The right panel shows the Monte Carlo simulation with 11.20 Gyr, that best fitted the data. The red labels illustrate the spread in mass, according to the models, ranging from $0.515 M_{\odot}$, at the top of the cooling sequence, which is consistent with spectroscopic results, to $0.817 M_{\odot}$ at the bottom.

function and colour-magnitude diagrams of their simulations of 47 Tuc, we could only compare our simulated luminosity function to the ones from García-Berro et al. (2014). In Fig. 15 we show, in the top panel, the luminosity function of our best fit model compared to the data. In the lower panel of Fig. 15 the luminosity function of the best fit model by García-Berro et al. (2014) presented in their Fig. 4, compared to the data. As García-Berro et al. (2014) did not use the proper motion correction, their luminosity function had a total area slightly larger than the one from our sample. So we normalised their luminosity function to the total number in our data. It is clear that our models present a very similar agreement to the data when compared to the models from García-Berro et al. (2014). One feature that must be emphasised is that, even though the effect is present in our models, neither the models nor the data of 47 Tuc present a clear crystallisation peak.

When we compare the white dwarf cooling data and the Monte Carlo simulation that best fits the data we find an excellent agreement, as can be seen in Fig. 16, for 47 Tuc. The spread in mass (red labels), according to the models, is ranging from $\sim 0.515 M_{\odot}$, at the top of the cooling sequence, which is consistent with spectroscopic results, to $\sim 0.817 M_{\odot}$ at the bottom. When compared to the models by García-Berro et al. (2014), our colour magnitude diagram presents an excellent agreement, also for the hotter white dwarf stars. We could not compare our luminosity function to the ones obtained by Hansen et al. (2013) because they do not show this important result in their paper. Also, as the colour-magnitude diagram of the simulations from Hansen et al. (2013) is not shown, we can not see if

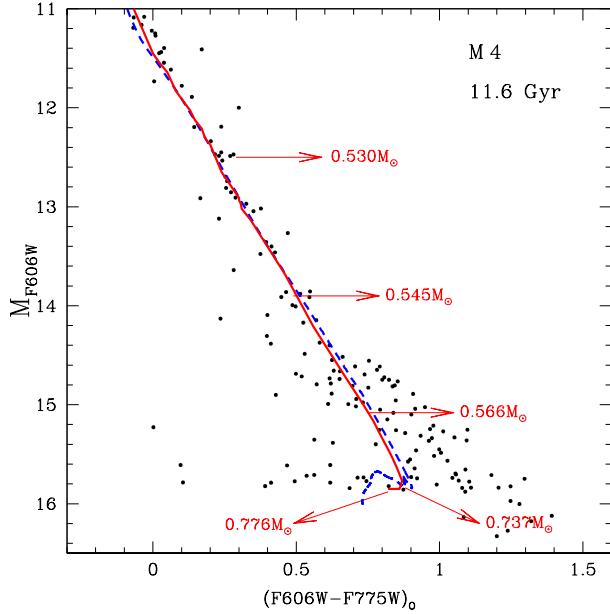


Figure 17. Our isochrone model (solid red line) over-plotted with the observed white dwarf cooling sequence of M4 using the age, distance modulus and reddening correction obtained by Richer et al. (2013). Also shown is the white dwarf isochrone obtained by Salaris et al. (2010) (dashed blue line), which points out the consistency between both models.

the observed blue turn feature is present in their models for 47 Tuc.

4.1.3 M4

With only 14 HST orbits obtained for M4, Bedin et al. (2009) were able to reach the blue turn of the white dwarf cooling sequence. The data obtained in filters F606W and F775W has poorer quality and much less stars, if compared with the data from NGC 6397 and 47 Tuc. The small number of stars along with the large scatter presented in the white dwarf cooling sequence prevents us from performing an analysis similar to the one we did for NGC 6397 and 47 Tuc. The chi-square analysis requires a minimum number of points to be reliable (Press et al. 2007), and that is not the case for this data.

Nevertheless, in order to compare our models to the data, in Fig. 17 we over-plotted the data using our isochrone model with 11.60 Gyr (solid red line), the age determined by Bedin et al. (2009), with the distance modulus and reddening from Richer et al. (2013). It is noticeable that the model reproduces the blue turn very well, even though the blue branch of our model is shorter than the data because the photometric scatter for these data is very high and currently the highest progenitor mass we have in our model, for the metallicity of M4, is $2.25 M_{\odot}$. This model shows that the range of masses of the white dwarf stars is between $\sim 0.527 M_{\odot}$ to $\sim 0.776 M_{\odot}$. Again, the mass at the top of the white dwarf cooling sequence is consistent with the results from spectroscopy (Moehler et al. 2004; Kalirai et al. 2009).

We also over-plotted a 11.6 Gyr white dwarf isochrone obtained by Salaris et al. (2010) (dashed blue line) to com-

pare with our model. Although Salaris et al. (2010) models have a wider blue branch, because the highest progenitor mass in their model is $\sim 6 M_{\odot}$, the shape of their model is completely consistent with ours and, also, Salaris et al. (2010) models show that the blue turn is due the increasing masses.

5 DISCUSSION

Our age determinations are consistent with those obtained by VandenBerg et al. (2013) using what they call the improved version of the ΔV_{TO}^{HB} method. They found 13.00 ± 0.25 Gyr for NGC 6397 and 11.75 ± 0.25 Gyr for 47 Tuc that, within the uncertainties, agree with our values. In addition, our age value for 47 Tuc is consistent, within the uncertainties, with the 12.0 ± 0.5 Gyr determined by García-Berro et al. (2014) also using the cooling sequence method. And our determination for NGC 6397 also agrees with the $12.8^{+0.50}_{-0.75}$ Gyr determined by Torres et al. (2015) using the white dwarf cooling sequence.

To demonstrate the effect of our age determinations on the age-metallicity relation, we show in Fig. 18 the age, determined through white dwarf cooling sequence, versus the metallicity for Galactic population, similar to what was done by Hansen et al. (2013). It is possible to see that M4 has an intermediate metallicity when compared to 47 Tuc and NGC 6397, and, apparently, also an intermediate age. This reinforces the age-metallicity relation stating that the metal-poor formed earlier than the metal-rich globular clusters.

The comparison between the white dwarf cooling data and the Monte Carlo model that best fits the data presents an excellent agreement, as can be seen in Figs. 8 and 11, for NGC 6397, and Figs. 14 and 16, for 47 Tuc. The turn to the blue is better reproduced for NGC 6397, if we compare to the one presented by Hansen et al. (2007), their Fig. 11, where their models did not fully reproduced the clump of stars blueward of the faint end of cooling sequence. However, the scattering in the model of 47 Tuc seems to be higher than the one from the data, indicating that the scatter of the artificial star tests could be overestimated. Also, the red offset problem is not corrected even when we include the photometric scatter in the models.

Our Monte Carlo Simulations do not include multiple star formation bursts, unresolved binaries or multiple populations. Thus, the small discrepancies between our models and the data may be related to the lack of those effects. We discuss more in the following paragraphs.

Torres et al. (2015) found a low value ($\sim 4\%$) for the binary fraction in NGC 6397, which is very similar to the $\sim 4.5\%$ fraction found for the main sequence stars by Ji & Bregman (2015). The latter authors also determined the binary fraction for 47 Tuc as being $\sim 3\%$, arguing that, for globular clusters, the binary fraction slowly decreases with dynamical age, i.e., above 10 relaxation times, there should be no clusters with binary fractions above 6%.

García-Berro et al. (2014) find that a burst of star formation for 47 Tuc occurred between 0.7 ± 0.5 Gyr and 1.0 ± 0.5 Gyr, depending on the distribution employed. Torres et al. (2015) also attempted to determine the burst of star formation for NGC 6397. However, their best fit obtained the duration of the burst of star formation as being

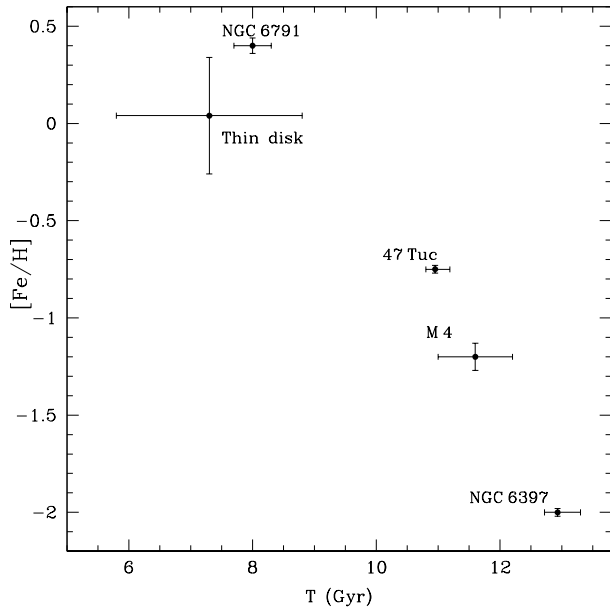


Figure 18. Age-metallicity relation based on ages determined with white dwarf cooling sequence and the metallicity for Galactic population determined from main sequence stars. The ages of NGC 6397 and 47 Tuc are the ones determined in the present work. The ages of NGC 6791 and the thin disk were taken from Hansen et al. (2013) and references therein. For M 4 the age is the one determined by Bedin et al. (2009).

$\Delta t = 3.3$ Gyr. They argued that, with the high accuracy photometric data obtained with Hubble Space Telescope, such an extended episode of star formation would be detectable in the colour-magnitude diagram of main sequence stars, which is not the case. So, they conclude that the photometric data available for the white dwarf stars of NGC 6397 is not appropriate for this kind of analysis and they adopt a initial burst of star formation as being 1.0 Gyr.

In Fig. 19 we show a comparison between the observed luminosity function from NGC 6397 to a simulated one with two bursts of star formation with 1 Gyr difference (11.93 Gyr and 12.93 Gyr). We notice that this model does not present a feature that is clearly present in the data: the crystallization peak. This feature is present in our single burst star formation model presented in Fig. 8. That could be an indication that the age difference between two bursts, if present, should be smaller than 1 Gyr for NGC 6397.

Milone et al. (2012) found that for certain filters, the photometry of 47 Tuc splits not only the main sequence in two branches, but also the sub-giant, red-giant regions and on the horizontal branch. Their results indicated that the differences between the two main sequences could be explained in terms of two stellar generations, one of them being formed by the primordial He, and O-rich/N-poor stars, and the other corresponding to a second generation population that was enriched in He and N but depleted in O. The He content would be $Y = 0.256$ for the primordial population and $Y = 0.272$ for the second generation. Hansen et al. (2013) accounted for He enrichment consistent with the one obtained by Milone et al. (2012), but they concluded that

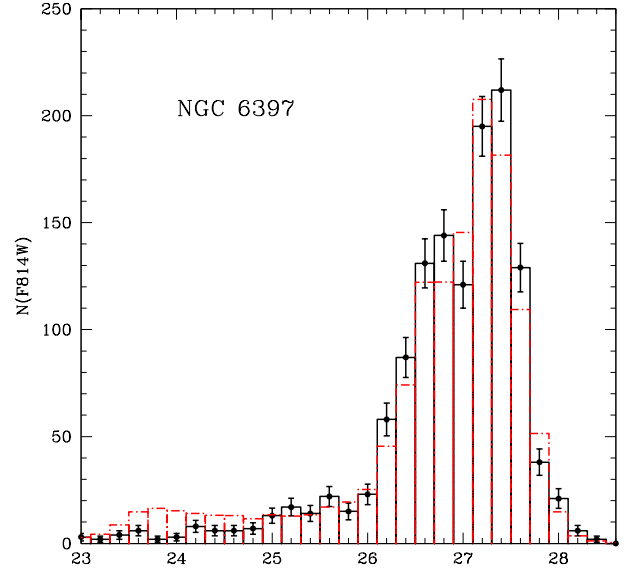


Figure 19. Comparison between the observed luminosity function from NGC 6397 (solid black line) to a simulated one (dashed red line) with two bursts of star formation with 1 Gyr difference (11.93 Gyr and 12.93 Gyr). The crystallization peak is not present in the model, indicating that the age difference between two bursts should be smaller than 1 Gyr for NGC 6397.

the resulting differences in the models do not lead to significant changes in the cooling age.

When we determine the distance modulus and reddening with the white dwarf stars hotter than 5500 K, our reddening determinations are systematically smaller than the ones determined with the main sequence fitting, with a $\Delta_{\text{colour}} \sim 0.07$. This could indicate that the white dwarf stars hotter than 5500 K are somehow slightly redder than the main sequence stars.

For NGC 6397 and 47 Tuc clusters our Monte Carlo simulations present a strong turn to the blue at the faint magnitudes, caused by increasing masses, and the temperature at this point is ~ 4300 K. The collision-induced absorption, as it is currently described (e.g. Borysow, Frommhold & Moraldi 1989; Borysow & Jørgensen 2000), would only be noticeable in infra-red colours ($M_K, J - K$), taking place at much lower temperatures, causing the second turn, but now to red colours as argued by Bono, Salaris & Gilmozzi (2013). They claim that, at fainter magnitudes ($M_{\text{bol}} \sim 16$), the white dwarf isochrone becomes populated by more massive white dwarf stars, and those are less blue because of the different cooling speed and onset of the collision-induced absorption, causing a red turn in the white dwarf cooling sequence for near infra-red isochrone models.

When we focus on the slope of the present day local mass function, we find that $\alpha = 2.17^{+0.34}_{-0.30}$ for NGC 6397, that is slightly different from the canonical $\alpha = 2.35$ from Salpeter (1955), and consistent with a top-heavy type, as has already been suggested by Richer et al. (2008) and references therein. In contrast, the value of $\alpha = 3.42^{+0.50}_{-0.46}$ obtained as the best fit to 47 Tuc data is very different from the canonical. However, it must be noted that we are analysing data from a

single region of the cluster. The very high α determined for 47 Tuc indicates a bottom heavy present day local mass function in that portion of the cluster, i.e., the present day local mass function of 47 Tuc is deficient in more massive white dwarf stars. Such a lack of massive white dwarf stars could be related to the diffusion due to gravitational relaxation that was detected for 47 Tuc by Heyl et al. (2015). By analysing the data from the core of 47 Tuc, Heyl et al. (2015) detected that the spatial distribution of young (less massive) white dwarf stars is significantly more centrally concentrated than the older (more massive) ones, indicating that the white dwarf distribution seems to be more radially diffuse with increasing age (Heyl et al. 2015). As the data we are using in our analysis is very close to the centre ($r \sim 8.8$ pc), while the tidal radius is $r_t \sim 52.0$ pc, a bottom heavy present day local mass function is another indicator of the lack of massive white dwarf stars near the centre of 47 Tuc.

A feature highlighted in Fig. 11 and Fig. 16 is that the models, built with the initial-to-final mass relation of Romero, Campos & Kepler (2015), show a spread in mass ranging from $\sim 0.525 M_\odot$, at the top of the cooling sequence, to $\sim 0.875 M_\odot$, for NGC 6397, and $\sim 0.520 M_\odot$ to $\sim 0.817 M_\odot$, for 47 Tuc. The mass at the truncation for NGC 6397 is significantly larger than the $\sim 0.62 M_\odot$ estimated by Hansen et al. (2007) for the same data. The models Hansen et al. (2007) used to determine the pre-white dwarf times attempted to take the effect of the metallicity into account. However, they considered as the white dwarf mass that at the first thermal pulse in the AGB. This approach, by not taking all the thermal pulses into account causes the major difference between the values of the final masses (Fig. 2).

Another point that should be emphasised is that our models that best fit the data lead to masses at the top of the white dwarf cooling sequence of $\sim 0.525 M_\odot$ for NGC 6397 and $\sim 0.520 M_\odot$ for 47 Tuc, that are consistent with the values found with spectroscopy of the brightest white dwarf stars in NGC 6397, NGC 6752 and M 4 ($\overline{M} = 0.53 \pm 0.03 M_\odot$, Moehler et al. 2004; $\overline{M} = 0.53 \pm 0.01 M_\odot$, Kalirai et al. 2009).

6 CONCLUSIONS

The first colour-magnitude diagrams of globular clusters down to the cutoff in the white dwarf cooling sequence exposed unprecedented features. One of these is the blue turn at magnitudes around $M_{\text{Bol}} \sim 14.7$ which was not well reproduced by single mass white dwarf models.

The effect of different model assumptions on the mass spread of the white dwarf stars and the importance of a consistent and detailed computation of their cooling evolution becomes clear when we compare the ages of NGC 6397 and 47 Tuc determined by Hansen et al. (2013) (11.70 Gyr and 9.90 Gyr), with those obtained from our best-fit isochrone models (12.93 Gyr and 10.95 Gyr). Our absolute ages for both clusters are higher and, the age difference between NGC 6397 and 47 Tuc is $1.98^{+0.44}_{-0.26}$ Gyr. This difference is consistent with that determined by Hansen et al. (2013) of 2.0 ± 0.5 Gyr. However, if we wanted to consider the distance modulus and reddening of the main sequence, the absolute

age of each cluster would change to 12.48 Gyr (NGC 6397) and 11.31 Gyr (47 Tuc), and the age deficit ($1.17^{+0.50}_{-0.31}$ Gyr) would be different than that by Hansen et al. (2013).

Also, the absolute ages we determined are consistent with the formation epochs of metal-poor and metal-rich globular clusters determined by Forbes et al. (2015). They inferred a mean formation epoch of globular clusters of $11.5^{+0.6}_{-1.2}$ Gyr for the metal-rich and, $12.2^{+0.2}_{-0.3}$ Gyr, for the metal-poor, if they all accreted from satellites, and $12.8^{+0.2}_{-0.4}$ Gyr, if they are all formed within the main host galaxy. When they apply a similar method to the Milky Way they find 10.7 Gyr for the metal-rich and 12.5-12.8 Gyr for the metal-poor depending on whether they formed in accreted satellites or within the main host galaxy. Additionally, Trenti, Padoan & Jimenez (2015) derived an average of old globular clusters as 13.00 ± 0.2 Gyr through cosmological simulations, which, again, is consistent with the age we determine for NGC 6397.

Even though the red offset problem does not interfere in the fitting—because we keep the reddening as a fixed parameter—the models that best fit the data still face the red offset problem, i.e., change in the slope of white dwarf cooling sequence after $M_{\text{Bol}} \sim 14.6$, that shows a trend for the models to be bluer than the data, indicating that the construction of models of white dwarf stars still have significant aspects that must be addressed in the future. The red offset problem is possibly related to partial mixing of H and He in the atmosphere of white dwarf stars and/or the lack of a better physical description of the collision-induced absorption. By running some tests in our models, we notice that the effect of a very small mixing of hydrogen and helium in the atmosphere of the ultra-cool white dwarf stars correct the slope of the models. However this still is an ongoing investigation. Also, the red offset is in the same direction as that of mismatches observed when isochrone models are compared to the coolest main sequence stars, indicating that this might be a common problem for stars with very low temperatures, i. e., opacities for the coolest stars. Also, there are no models calculated with the newest collision-induced absorption opacities (Abel et al. 2012), so it is still an open question if they will help to solve the red offset problem.

We determined a very high value of α for 47 Tuc, i.e., a bottom heavy present day local mass function in that portion of the cluster. Heyl et al. (2015) explained the lack of massive white dwarf stars near the centre of 47 Tuc by the diffusion due to gravitational relaxation. The data we use in our analysis is very close to the centre of the cluster so, a bottom heavy present day local mass function is another indicator of the lack of massive white dwarf stars near the centre of 47 Tuc. For NGC 6397 we find an α consistent with a top-heavy type, in line with the analysis by Richer et al. (2008) and references therein.

Another important feature highlighted in our analysis is the crystallisation peak, that is clearly visible in both, the data and the model, for NGC 6397 at F606W \sim 28, is not prominent for 47 Tuc. For this cluster, neither the models nor the data present a clear crystallisation peak.

ACKNOWLEDGEMENTS

The authors would like to thank the anonymous referee for important suggestions that helped improve the manuscript. The authors would like to thank B.M.S. Hansen and H. B. Richer for their suggestions, for sending the photometric data and the artificial star tests of NGC 6397. F.C. would like to thank J.S. Kalirai for sending the artificial star tests of 47 Tuc. Partial financial support for this research comes from CNPq and PRONEX-FAPERGS/CNPq (Brazil). This work was supported in part by the NSERC Canada and by the Fund FRQ-NT (Québec). M.H.M. and D.E.W. gratefully acknowledge the support of the NSF under grants AST-0909107 and AST-1312983. L.R.B. acknowledge PRIN-INAFA 2012 funding under the project entitled: “The M4 Core Project with Hubble Space Telescope”.

References

Abel, Martin; Frommhold, Lothar; Li, Xiaoping; Hunt, Katharine L. C. 2012, JChPh, 136, 431

Althaus, L.G.; Serenelli, A.M.; Córscico, A.H. & Montgomery, M.H. 2003, A&A, 404, 593

Althaus, L. G.; Serenelli, A. M.; Panei, J. A.; Córscico, A. H.; García-Berro, E. & Scóccola, C. G. 2005, A&A, 435, 631

Althaus, L. G.; Camisassa, M. E.; Miller Bertolami, M. M.; Córscico, A. H. & García-Berro, E. 2015, A&A, 576, 9

Anderson, J.; King, I. R.; Richer, H. B.; Fahlman, G. G.; Hansen, B. M. S.; Hurley, J.; Kalirai, J. S.; et al. 2008, AJ, 135, 2114

Bedin, L. R.; Piotto, G.; King, I. R. & Anderson, J. 2003, AJ, 126, 247

Bedin, L. R.; Piotto, Giampaolo; A., Jay; Cassisi, S.; King, I. R.; Momany, Y. & Carraro, G. 2004, ApJ, 605L, 125

Bedin, L. R.; Salaris, M.; Piotto, G.; King, I. R.; Anderson, J.; Cassisi, S. & Momany, Y. 2005, ApJ, 624, 45

Bedin, L. R.; Piotto, G.; Carraro, G.; King, I. R. & Anderson, J. 2006, A&A, 460, L27

Bedin, L. R.; King, I. R.; Anderson, J.; Piotto, G.; Salaris, M.; Cassisi, S. & Serenelli, A. 2008a, ApJ, 678, 1279

Bedin, L. R.; Salaris, M.; Piotto, G.; Cassisi, S.; Milone, A. P.; Anderson, J. & King, I. R. 2008b, ApJ, 679L, 29

Bedin, L. R.; Salaris, M.; Piotto, G.; Anderson, J.; King, I. R.; & Cassisi, S. 2009, ApJ, 678, 1279

Bedin, L. R.; Salaris, M.; King, I. R.; Piotto, G.; Anderson, J.; & Cassisi, S. 2010, ApJ, 708, 32

Bedin, L. R.; Salaris, M.; Anderson, J.; Cassisi, S.; Milone, A. P.; Piotto, G.; King, I. R. & Bergeron, P. 2015, MNRAS, 448, 1779

Bellini, A.; Anderson, J.; Salaris, M.; Cassisi, S.; Bedin, L. R.; Piotto, G. & Bergeron, P. 2013, ApJ, 769L, 32

Bergeron, P., Wesemael, F., Fontaine, G. & Liebert, J. 1990, ApJ, 351, L21

Bergeron, P.; Saumon, D. & Wesemael, F. 1995, ApJ, 443, 764

Bergeron, P.; Leggett, S. K. & Ruiz, M. T. 2001, ApJS, 133, 413

Bergeron, P. & Leggett, S. K. 2002, ApJ, 580, 1070

Bonatto, C.; Bica, E.; Ortolani, S. & Barbuy, B. 2007, MNRAS, 381L, 45

Bono, G.; Salaris, M. & Gilmozzi, R. 2013, A&A, 549A, 102

Borysow, A.; Frommhold, L. & Moraldi, M. 1989, ApJ, 336, 495

Borysow, A.; Græe Jørgensen, U. 2000, ASPC, 212, 173

Cardelli, J.A.; Clayton, G.G. & Mathis, J.S. 1989, ApJ, 345, 245

Castanheira, B. G. & Kepler, S. O. 2008, CoAst, 157, 294

Castanheira, B. G. & Kepler, S. O. 2009, JPhCS, 172a, 2068

Chabrier, G. 2003, PASP, 115, 763

Chen, E. Y. & Hansen, B. M. S. 2014, MNRAS, 444, 2525

Chen, Y.; Girardi, L.; Bressan, A.; Marigo, P.; Barbieri, M. & Kong, X. 2011, MNRAS, 413, 2827

Clemens, J. C. 1993, Baltic Astronomy, 2, 407

D’Antona, F. & Mazzitelli, I. 1979, A&A, 74, 161

D’Antona, F.; Bellazzini, M.; Caloi, V.; Fusi Pecci, F.; Galilei, S. & Rood, R. T. 2005, ApJ, 611, 871

Davis, D. S.; Richer, H. B.; Anderson, J.; Brewer, J.; Hurley, J.; Kalirai, J. S.; Rich, R. M. & Stetson, P. B. 2008, AJ, 135, 2155

Davis, D. S.; Richer, H. B.; Rich, R. M.; Reitzel & Kalirai, J. S. 2009, ApJ, 705, 398

Deloye, C. J. & Bildsten, L. 2002, ApJ, 580, 1077

Doherty, C. L.; Gil-Pons, P.; Siess, L.; Lattanzio, J. C. & Lau, H. H. B. 2015, MNRAS, 446, 2599

Dotter, A.; Sarajedini, A.; Anderson, J.; Aparicio, A.; Bedin, L. R.; Chaboyer, B.; Majewski, S.; Marín-Franch, A.; et al. 2010, ApJ, 708, 698

Fisherman, G. S. 1995, Monte Carlo: Concepts, Algorithms, and Applications, 1st edn, Springer series in operations research, New York

Fontaine, G. & Michaud, G. 1979, ApJ, 231, 826

Fontaine, G.; Brassard, P. & Bergeron, P. 2001, PASP, 113, 409

Forbes, D. A.; Pastorello, N.; Romanowsky, A. J.; Usher, C.; Brodie, J.P. & Strader, J. 2015, arXiv:1506.06820

Frommhold, L. 2001, Encyclopedia of Physical Science and Technology, 3, 269

García-Berro, E., Torres, S.; Althaus, L. G.; Renedo, I.; Lorén-Aguilar, P.; Córscico, A. H.; Rohrmann, R.; Salaris, M. & Isern, J. 2010, Nature, 465, 194

García-Berro, E.; Torres, S.; Althaus, L. G.; Miller Bertolami, M. M. 2014, A&A, 571, A56

Groenewegen, M. A. T., Sloan, G. C., Soszyński, I., & Petersen, E. A. 2009, A&A, 506, 1277

Hansen, B. M. S. 1998, Nature, 394, 860

Hansen, B. M. S.; Richer, H. B.; Fahlman, G. G.; Stetson, P. B.; Brewer, J.; Currie, T.; Gibson, B. K.; Ibata, R.; et al. 2004, ApJS, 155, 551

Hansen, B. M. S.; Anderson, J.; Brewer, J.; Dotter, A.; Fahlman, G. G.; Hurley, J.; Kalirai, J.; King, I.; et al. 2007, ApJ, 671, 380

Hansen, B. M. S.; Kalirai, J. S.; Anderson, J.; Dotter, A.; Richer, H. B.; Rich, R. M.; Shara, M. M.; Fahlman, et al. 2013, Nature, 500, 51

Harris, W.E. 1996, AJ, 112, 1487

Harris, G. J.; Lynas-Gray, A. E.; Miller, S. & Tennyson, J. 2004, ApJ, 617L, 143

Heyl, J. S.; Richer, H.; Anderson, J.; Fahlman, G.; Dotter, A.; Hurley, J.; Kalirai, J.; Rich, R. M.; et al. 2012, ApJ, 761, 51

Heyl, J.; Richer, H. B.; Antolini, E.; Goldsbury, R.; Kalirai,

- J.; Parada, J. & Tremblay, P.-E 2015, ApJ, 804, 53
- Horowitz, C.J., Schneider, A.S., & Berry, D.K. 2010, Physical Review Letters, 104, 231101
- Hurley, J. R. & Shara, M. M. 2003, ApJ, 589, 179
- Ibeling, D. & Heger, A. 2013, ApJ, 765L, 43
- Ji, J. & Bregman, J. N. 2015, ApJ, 807, 32
- Kalirai, J. S.; Richer, H. B.; Reitzel, D.; Hansen, B. M. S.; Rich, R. M.; Fahlman, G. G.; Gibson, B. K.; von Hippel, T. 2005, ApJ, 618L123
- Kalirai, J. S.; Anderson, J.; Richer, H. B.; King, I. R.; Brewer, J. P.; Carraro, G.; Davis, S. D.; Fahlman, G. G.; et al. 2007, ApJ, 657L, 93
- Kalirai, J. S.; Hansen, B. M. S.; Kelson, D. D.; Reitzel, D. B.; Rich, R. M.; Richer, H. B. 2008, ApJ, 676, 594
- Kalirai, J. S.; Saul, D., D.; Richer, H. B.; Bergeron, P.; Catelan, M.; Hansen, B. M. S.; Rich, R. Michael 2009, ApJ, 705, 408
- Kalirai, J. S.; Richer, H. B. 2010, RSPTA, 368, 755
- Kalirai, J. S.; Richer, H. B.; Anderson, J.; Dotter, A.; Fahlman, G. G.; Hansen, B. M. S.; Hurley, J.; King, I. R.; et al. 2012, ApJ, 143, 11
- Kalirai, J. S. 2013, MmSAI, 84, 58
- Kalirai, J. S., Marigo, P., & Tremblay, P.-E. 2014, ApJ, 782, 17
- Kilic, M.; Leggett, S. K.; Tremblay, P.-E.; von Hippel, Ted; Bergeron, P.; Harris, H. C.; Munn, J. A.; Williams, K. A.; et al. 2010, ApJS, 190, 77
- Koester, D. 1976, A&A, 52, 415
- Koester, D. & Kepler, S. O. 2015, arXiv:1509.08244
- Kowalski, P. M. & Saumon, D. 2006, ApJ, 651, L137
- Kowalski, P. M. 2007, A&A, 474, 491
- Limoges, M.-M.; Bergeron, P.; Lépine, S. 2015, ApJS, 219, 19
- Miller Bertolami, M. M., Althaus, L. G., & García-Berro, E. 2013 ApJL, 775, L22
- Milone, A. P.; Piotto, G.; Bedin, L. R.; King, I. R.; Anderson, J.; Marino, A. F.; Bellini, A.; Gratton, R.; et al. 2012, ApJ, 744, 58
- Moehler, S.; Koester, D.; Zoccali, M.; Ferraro, F. R.; Heber, U.; Napiwotzki, R. & Renzini, A. 2004, A&A, 420, 515
- Moehler, S.; Bono, G. 2008, arXiv:0806.4456
- Paxton, B.; Bildsten, L.; Dotter, A.; Herwig, F.; Lesaffre, P.; Timmes, F. 2011, ApJS, 192, 3
- Paxton, B.; Cantiello, M.; Arras, P.; Bildsten, L.; Brown, E. F.; Dotter, A.; Mankovich, C.; Montgomery, M. H.; et al. 2013, ApJ, 208, 4
- Piotto, G.; Milone, A. P.; Bedin, L. R.; Anderson, J.; King, I. R.; Marino, A. F.; Nardiello, D.; Aparicio, A.; et al. 2015, AJ, 149, 91
- Press, W. H.; Teukolsky, S. A.; Vetterling, W. T. & Flannery, B. P 2007, Numerical Recipes: The Art of Scientific Computing, 3rd edn, Cambridge University Press., Cambridge
- Reimers, D. 1977, A&A, 61, 217
- Renedo, I.; Althaus, L. G.; Miller Bertolami, M. M.; Romero, A. D.; Córscico, A. H.; Rohrmann, R. D. & García-Berro, E. 2010, ApJ, 717, 183
- Richer, H. B.; Anderson, J.; Brewer, J.; Davis, S.; Fahlman, G. G.; Hansen, B. M. S.; Hurley, J.; Kalirai, J. S.; et al. 2006, Science, 313, 936
- Richer, H. B.; Dotter, A.; Hurley, J.; Anderson, J.; King, I. R.; Davis, S.; Fahlman, G. G.; Hansen, B. M. S.; et al. 2008, AJ, 135, 2141
- Richer, H. B.; Goldsbury, R.; Heyl, J.; Hurley, J.; Dotter, A.; Kalirai, J. S.; Woodley, K. A.; Fahlman, G. G.; et al. 2013, ApJ, 778, 104
- Rohrmann, R. D., Althaus, L. G., García-Berro, E., Córscico, A. H., & Miller Bertolami, M. M. 2012, A&A, 546, A119
- Romero, A. D.; Córscico, A. H.; Althaus, L. G.; Kepler, S. O.; Castanheira, B. G. & Miller Bertolami, M. M. 2012, A&AS, 145, 451
- Romero, A. D.; Kepler, S. O.; Córscico, A. H.; Althaus, L. G. & Fraga, L. 2013, ApJ, 779, 58
- Romero, A. D.; Campos, F. & Kepler, S. O. 2015, MNRAS, 450, 3708
- Salaris, M., Serenelli, A., Weiss, A., & Miller Bertolami, M. 2009, ApJ, 692, 1013
- Salaris, M.; Cassisi, S.; Pietrinferni, A.; Kowalski, P. M. & Isern, J. 2010, ApJ, 716, 1241
- Salpeter, E. E. 1955, ApJ, 121, 161
- Saumon, D. & Jacobson, S. B. 1999, ApJ, 790, 50
- Saumon, D.; Holberg, J. B.; Kowalski, P. M. 2014, ApJ, 511, L107
- Torres, S.; García-Berro, E.; Althaus, L. G. & Camisassa, M. E. 2015, A&A, arXiv:1507.08806
- Tremblay, P.-E., & Bergeron, P. 2008, ApJ, 672, 1144
- Tremblay, P.-E.; Bergeron, P.; Kalirai, J. S. & Gianninas, A. 2010, ApJ, 712, 1345
- Tremblay, P.-E.; Ludwig, H.-G.; Steffen, M. & Freytag, B. 2013, A&A, 552A, 13
- Tremblay, P.-E.; Ludwig, H.-G.; Freytag, B.; Fontaine, G.; Steffen, M. & Brassard, P. 2015, ApJ, 799, 142
- Trenti, M.; Padoan, P. & Jimenez, R. 2015, arXiv:1502.02670v2
- VandenBerg, D. A.; Brogaard, K.; Leaman, R. & Casagrande, L. 2013, ApJ, 775, 134
- Vassiliadis, E. & Wood, P. R. 1993, ApJ, 413, 641
- Vauclair, G. & Reisse, C. 1977, A&A, 61, 415
- Weiss, A., & Ferguson, J. W. 2009, A&A, 508, 1343
- Williams, K. A., Bolte, M., & Koester, D. 2009, ApJ, 693, 355
- Winget, D. E.; Kepler, S. O.; Campos, F.; Montgomery, M. H.; Girardi, L.; Bergeron, P.; Williams, K. 2009, ApJ, 693L, 6
- Winget, D. E.; Montgomery, M. H.; Kepler, S. O.; Campos, F. & Bergeron, P. 2010, AIPC, 1273, 146

This paper has been typeset from a \LaTeX file prepared by the author.